Parameterization Sensitivity and Instability Characteristics of the Maximum Sustainable Heat Flux Framework for Predicting Turbulent Collapse

Amber M. Holdsworth, Tim Rees and Adam Monahan

September 2016

Parameterization Sensitivity and Instability Characteristics of the Maximum Sustainable Heat Flux Framework for Predicting Turbulent Collapse

AMBER M. HOLDSWORTH, TIM REES, AND ADAM H. MONAHAN

School of Earth and Ocean Sciences, University of Victoria, Victoria, British Columbia, Canada

(Manuscript received 19 February 2016, in final form 27 May 2016)

ABSTRACT

A maximum sustainable heat flux (MSHF) framework for the collapse of turbulence in the stable boundary layer has been previously studied using a one-dimensional model of Couette flow with parameterized turbulent fluxes. This study further investigates the stability properties of this model and assesses the robustness of the MSHF framework for predicting turbulent collapse to the choice of turbulence parameterization. The dynamic stability properties of the system are studied through numerical analysis of linearized equations of motion, and these results are compared with numerical solutions of the fully nonlinear system. While the MSHF mechanism and the qualitative features of the equilibrium structure are robust to changes in turbulence parameterizations, important quantitative differences between the models are found. While the equilibrium structures for Businger–Dyer-type stability functions are independent of the roughness length z_0, all of the other relations show a strong dependence on z_0 with regard to their shapes and the value of the MSHF. Equilibrium curves for some of the parameterizations exhibit multiple extrema, and transitions between stable and unstable regimes occur at extrema of the equilibrium curves in parameter space. Along the unstable branch(es), the Couette flow model has only a single unstable mode for all turbulence parameterizations considered. The MSHF framework is qualitatively robust to the choice of parameterization, but its use to predict the collapse of turbulence in the SBL is quantitatively sensitive to the turbulence scheme, especially for small values of z_0.

1. Introduction

The atmospheric boundary layer (ABL) is the lowermost part of the atmosphere that is directly influenced by Earth's surface and across which turbulent transports exchange momentum, energy, and matter between the surface and the free atmosphere. Under conditions of clear skies, in the evening net surface longwave emission exceeds shortwave absorption, and the ground surface becomes colder than the overlying atmosphere. Turbulence in the resulting stable boundary layer (SBL) can then only be maintained by mechanical generation of turbulence kinetic energy (TKE). The evolution of stratification with time is determined by how efficiently turbulence can transport energy toward the surface relative to how rapidly it is lost by radiative fluxes. Such stable boundary layers can also form during fair skies and weak pressure gradients in basins, in local depressions, and in valleys with weak down-valley slopes (Mahrt 2014). The longest-enduring stable boundary layer is found during the polar night, which can last over 80 days (Grachev et al. 2005). Near-calm conditions can be associated with low surface temperatures, an accumulation of pollutants near the ground, and the formation of dense fog (Mahrt 2011).

Understanding and modeling the SBL is essential for both regional and global atmospheric models. Regional models are used to model, for example, pollutant dispersal (Nappo 1991; Arya 1999; Salmond and McKendry 2005), wind speed power and distribution for wind power assessments (Petersen et al. 1998), and the variability and extremes of near-surface winds (He et al. 2010; Monahan et al. 2011; He et al. 2012). For larger-scale models, such as numerical weather prediction or global climate models, an accurate representation of turbulent mixing is necessary to model the near-surface wind, temperature, and humidity. In particular, changes

Corresponding author address: Amber Holdsworth, School of Earth and Ocean Sciences, University of Victoria, P.O. Box 3065 STN CSC, Victoria BC V8W 3V6, Canada.
E-mail: amhold@uvic.ca

DOI: 10.1175/JAS-D-16-0057.1

in turbulent mixing may impact the representation of surface temperature extremes, fog, and clouds (Holtslag et al. 2013). All of these models require turbulence parameterizations, as physically relevant dynamics occur on scales of motion that are smaller than the grid scales can capture.

Both modeling and observational studies indicate that the interplay between the suppression of turbulence due to static stability and the mechanical generation of turbulence due to wind shear gives rise to multiple stability regimes within the stable boundary layer. The simplest classification scheme distinguishes the weakly stable boundary layer (WSBL) from the very stable boundary layer (VSBL) (Webb 1970; Walters et al. 2007; Mahrt 1998a, 2014). Weakly stable conditions occur in the presence of moderate to strong pressure gradients or cloudy skies and are characterized by the presence of continuous (if weak) turbulent mixing. Classic Monin–Obukhov similarity theory (MOST) generally holds in the WSBL (Mahrt 1998a; Grachev et al. 2005; Pahlow et al. 2001; Mahrt 2014). In contrast, a VSBL typically occurs in the presence of weak pressure gradients or clear skies (with strong surface radiative cooling), and turbulence can weaken to the point of collapse. Although turbulence may never completely cease in the VSBL, the scales of motion become small enough that the flow near the surface can decouple from the overlying atmosphere and MOST fails (Derbyshire 1999; Banta et al. 2007; Williams et al. 2013; Mahrt 2011; Optis et al. 2015).

As local stability parameters, such as the Richardson number (Ri), tend to be lower in the WSBL and higher in the VSBL, attempts have been made to define a transitional Richardson number that separates the two regimes (Mahrt 2014). Specifically, a so-called critical Richardson number (Ri_c) above which turbulence collapses has been sought out. The existence of such a value is debated (Holtslag and De Bruin 1988; Beljaars and Holtslag 1991), and if it exists, its value is highly uncertain (Fernando and Weil 2010). Other authors have emphasized the need for additional metrics to separate the regimes (Van de Wiel et al. 2002; Grachev et al. 2005; Monahan et al. 2015). More recent studies have argued that the collapse of turbulence is best interpreted in terms of the maximum sustainable downward heat flux (MSHF) (Van de Wiel et al. 2007, 2012b; Van Hooijdonk et al. 2015).

The existence of a maximum sustainable heat flux can be understood by considering the two factors that determine the heat flux: the strength of the temperature gradient and the intensity of turbulence (De Bruin 1994; Malhi 1995; Van Hooijdonk et al. 2015). In near-neutral conditions, the heat flux is weak because of the small temperature gradient, while in strongly stable conditions the heat flux is weak because turbulent transports are suppressed. For a given wind shear, there is an optimal combination of the turbulent intensity and the temperature gradient that gives rise to a maximum possible sensible heat flux.

Normally, stability analyses in fluid motion study the transition from laminar to turbulent flow. The primary focus of our analysis will be the more general dynamical systems concept of linear stability of equilibria, assessing the response of the model under consideration to small perturbations around equilibrium states corresponding to turbulent flows. We will refer to stability in the first, more restricted, sense as *hydrodynamic stability* and the more general sense simply as stability.

We will investigate the stability properties of the equilibrium states of Couette flow for different parameterizations of the turbulent fluxes. As first noted by Taylor (1971), the existence of an MSHF implies the existence of two equilibrium surface stresses for a specified surface heat flux (below the MSHF). Taylor's hypothesis that one of the solutions was stable and the other unstable was confirmed analytically for Couette flow with turbulent fluxes parameterized using a Businger–Dyer-type similarity function by Van de Wiel et al. (2007). The equilibrium state at which the stability properties of the linearized dynamics changed from stable to unstable was shown to correspond to the MSHF state. Van de Wiel et al. (2007) used numerical simulations of the time-dependent problem to show that one branch of the equilibrium curve was stable while the other was unstable.

Businger–Dyer-type parameterizations are known to be decreasingly accurate as stratification increases, and other flux parameterizations exist (e.g., Webb 1970; Hicks 1976; Clarke 1970; Holtslag and De Bruin 1988; Chenge and Brutsaert 2005; Brown et al. 2008; Delage 1997). As these parameterizations are obtained as empirical fits to datasets with large scatter, none of these parameterizations is expected to be absolutely correct, and qualitative features of the MSHF mechanism for turbulent collapse should be robust to changes in parameterization for this mechanism to be relevant to the atmospheric SBL. In this study, we will explore several of the available parameterizations to answer the question of whether the MSHF framework is sensitive to the choice of model.

Using data from the Royal Netherlands Meteorological Institute (KNMI) Cabauw observatory, Monahan et al. (2015) provided evidence of two distinct states of the SBL, corresponding to the stable and unstable branches of the Couette model equilibrium curves found by Van de Wiel et al. (2007). Roughly half of the

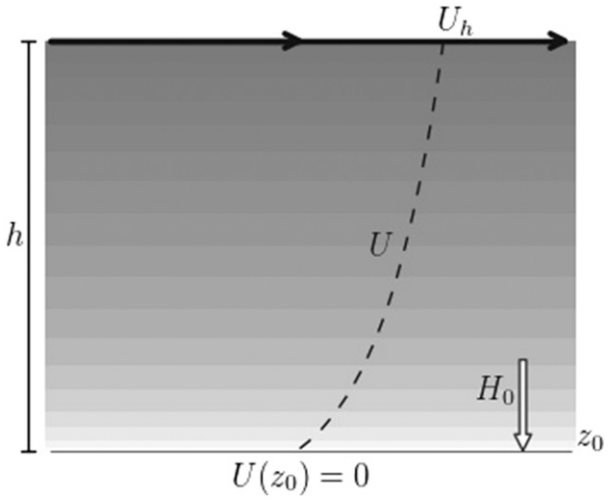

FIG. 1. Schematic diagram of the 1D Couette flow model. The lower boundary is fixed, and the upper boundary is constantly moving. The temperature profile is shaded in grayscale.

observed states fell along the unstable branch. The population of the unstable branch motivates a more thorough analysis of the stability properties of the equilibrium curve of the Couette flow model. In this study, we extend the results of Van de Wiel et al. (2007) to directly analyze the linear stability of equilibria for a range of turbulent flux parameterizations by numerically computing the eigenstructure of the linearized operator.

This paper is organized as follows. In section 2 we describe the Couette flow model, including the Richardson number–dependent parameterizations of turbulent viscosity and diffusivity. The framework for the equilibrium and linear stability analyses is presented in section 3. Results of numerically computed equilibrium curves and linear stability analysis are presented in section 4. Conclusions and discussion appear in section 5.

2. The Couette flow model

Following Van de Wiel et al. (2007), we consider a horizontally homogeneous, one-dimensional Couette flow model in which momentum and temperature tendencies result only from turbulent flux convergence. The Coriolis effect, pressure gradient force, radiative flux divergence, and molecular viscosity/diffusivity are neglected for simplicity. In particular, we neglect the existence of a molecular boundary layer that becomes relevant when the surface is so smooth that the viscous sublayer is actually deeper than the roughness elements. A schematic diagram for our model of wind speed U and temperature T in the SBL is shown in Fig. 1. The height of the upper boundary is fixed at $z = h$, where the wind speed U_h and temperature T_h are constant in time. The bottom of the model domain is at the momentum roughness length z_0. The no-slip boundary condition $[U(z_0) = 0]$ is implemented along with a specified constant surface heat flux H_0. Basu et al. (2008) argued that any model of the stable boundary layer that uses a prescribed sensible heat flux will only be able to capture the near-neutral or weakly stable regimes. Since our model simply examines the transition from the WSBL to the VSBL and does not model the VSBL directly, the use of this boundary condition is justified.

The velocity upper boundary condition was motivated in Van de Wiel et al. (2012b) by the observation that near-surface winds tend to weaken in the evening, while the flow above the nocturnal boundary layer tends to accelerate as a result of inertial effects. At an intermediate altitude, decameters above the ground, the magnitude of the wind remains approximately constant. This point was denoted the velocity crossing point (CP) by Van de Wiel et al. (2012b). At Cabauw, the altitude of the CP is observed to be about 40 m (Van de Wiel et al. 2012a). Thus, there is reason to believe that the Couette flow model can provide a useful first approximation even though it represents a dramatic simplification of the dynamics of the SBL.

The governing equations of the Couette system are

$$\partial_t U = \frac{1}{\rho}\,\partial_z \tau \quad \text{and} \tag{1}$$

$$\partial_t T = -\frac{1}{\rho c_p}\,\partial_z H, \tag{2}$$

where H is the turbulent heat flux and the turbulent stress is defined by $\tau = -\rho\overline{u'w'}$ for horizontal (u) and vertical (w) wind velocities. Turbulence is modeled by using a local closure, which assumes that the nonlocal transport terms are small under stably stratified conditions. Hence, turbulent fluxes are parameterized by

$$\frac{\tau}{\rho} = K_m \partial_z U \quad \text{and} \tag{3}$$

$$\frac{H}{\rho c_p} = -K_h \partial_z T, \tag{4}$$

with turbulent viscosity and diffusivity $K_{m,h} = l_n^2 |\partial_z U| f_{m,h}(\mathrm{Ri})$, where $l_n = \kappa z$. The influence of stratification and shear on turbulence intensity is expressed by the functions $f_{m,h}$ in terms of the gradient Richardson number and is given by

$$\mathrm{Ri} = \frac{g}{T_h}\,\frac{\partial_z T}{(\partial_z U)^2}. \tag{5}$$

In equilibrium, the turbulent fluxes are constant from $z = z_0$ to $z = h$. This constant flux layer can be described

TABLE 1. Stability functions for momentum f_m and heat f_h. The similarity functions $\phi_{m,h}$ are related to the stability functions $f_{m,h}$ through Eqs. (8).

Businger et al. (1971)	$\phi_{m,h}(\zeta) = 1 + \alpha\zeta$, $f_{m,h}(\mathrm{Ri}) = (1 - \alpha\mathrm{Ri})^2$	$\alpha = 5$
Holtslag and De Bruin (1988)	$\phi_{m,h}(\zeta) = 1 + a\zeta + b\zeta(1 + c - d\zeta)e^{-d\zeta}$	$a = 0.7$, $b = 0.75$, $c = 5$, $d = 0.35$
Beljaars and Holtslag (1991) (ECMWF)	$\phi_m(\zeta) = 1 + a\zeta + b\zeta(1 + c - d\zeta)e^{-d\zeta}$	$a = 1$, $b = 2/3$, $c = 5$, $d = 0.35$
	$\phi_h(\zeta) = 1 + \zeta a\left(1 + \frac{2}{3}\zeta\right)^{1/2} + b\zeta(1 - d\zeta + c)e^{-d\zeta}$	
Brown et al. (2008) (UKMO)	$f_{m,h}(\mathrm{Ri}) = \begin{cases} (1 - \alpha\mathrm{Ri})^2 & 0 \le \mathrm{Ri} \le 0.1 \\ \left(\frac{1}{20\mathrm{Ri}}\right)^2 & \mathrm{Ri} \ge 0.1 \end{cases}$	$\alpha = 5$

by MOST with the caveat that this theory may break down in the presence of very strong stratifications (Mahrt 1998b). MOST implies that the dimensionless wind shear and temperature gradients are given by the following universal functions of $\zeta = z/L$:

$$\phi_m(\zeta) = \frac{kz}{u_*}\partial_z U \quad \text{and} \tag{6}$$

$$\phi_h(\zeta) = \frac{z}{T_*}\partial_z T, \tag{7}$$

with the Obukhov length $L = \rho c_p u_*^3 T_h / H_0 \kappa g$ and $T_* = -H_0/\rho c_p u_*$, where $\kappa = 0.4$ is the von Kármán constant, $c_p = 1005\,\mathrm{J\,kg^{-1}\,K^{-1}}$ is the specific heat at a constant pressure, $\rho = 1.2\,\mathrm{kg\,m^{-3}}$ is the density of the air, and $g = 9.81\,\mathrm{m\,s^{-2}}$ is the gravitational acceleration. By definition $\tau/\rho = u_*^2$ and $H/\rho c_p = u_* T_*$. The dependence of the turbulence on stratification and shear can be expressed either in terms of the similarity functions $\phi_{m,h}(\zeta)$ or the stability functions $f_{m,h}(\mathrm{Ri})$, which are related by

$$f_m(\mathrm{Ri}_{\mathrm{eq}}) = \phi_m^{-2}(\zeta) \quad \text{and}$$
$$f_h(\mathrm{Ri}_{\mathrm{eq}}) = \phi_m^{-1}(\zeta)\phi_h^{-1}(\zeta). \tag{8}$$

While MOST predicts that the similarity functions should be universal, it does not predict their functional form. Many different forms of $\phi_{m,h}(\zeta)$ and $f_{m,h}(\mathrm{Ri})$ have appeared in the literature. The simplest are the Businger–Dyer-type stability functions $\phi_{m,h}(\zeta) = 1 + \alpha\zeta$ (Businger et al. 1971), such as were used in Van de Wiel et al. (2007, 2012a,b). Equations (8) can be used to find explicit expressions for $f_{m,h}(\mathrm{Ri})$ for Businger–Dyer-type stability functions (Table 1). Many different values of the constant α have been suggested in the literature, ranging from 2 (Pruitt et al. 1973) to 12 (Delage 1997). It is widely accepted that the Businger–Dyer-type stability functions $\phi_{m,h}(\zeta)$ are not appropriate for $z/L \gtrsim 1$ (Carson and Richards 1978; Howell and Sun 1999; Nieuwstadt 1984).

To assess the robustness of the MSHF framework for predicting the collapse of turbulence to the parameterizations of the turbulent fluxes, we examine four sets of stability functions. Their functional forms are given explicitly in Table 1 and are plotted in Fig. 2 alongside the similarity functions. The various stability function formulations have been proposed based on empirical fits to available data (e.g.,Webb 1970; Businger et al. 1971; Dyer 1974; Hicks 1976; Clarke 1970; Holtslag and De Bruin 1988; Chenge and Brutsaert 2005; Brown et al. 2008). However, flux observations in the very stable regime are subject to large variability and problems with sampling (Nieuwstadt 1984; Mahrt 1985), so it is difficult to ascertain empirically which function is most appropriate. Some of the relations imply the existence of an Ri_c (Businger et al. 1971; Brown et al. 2008; Holtslag and De Bruin 1988) above which u_* and H vanish. Because the existence of an Ri_c is still an open question, we examine both functions that imply an Ri_c and those that do not.

Andreas (2002) reviewed various stability functions used to model the stably stratified surface layer over snow and ice. They examined the characteristics of seven different sets of stability functions, including three of the functions presented in Table 1 (Businger et al. 1971; Holtslag and De Bruin 1988; Beljaars and Holtslag 1991). Assuming the existence of a critical Richardson number and that the turbulent Prandtl number $\mathrm{Pr}_t \equiv K_m(\zeta)/K_h(\zeta) = \phi_h(\zeta)/\phi_m(\zeta)$ should be equal to one, they concluded that the Holtslag and De Bruin (1988) functions were best suited to modeling in polar regions. To the contrary, many observational studies find that the transport mechanisms for heat and momentum differ in very stable conditions ($\phi_h > \phi_m$) (Hicks 1976; Kondo et al. 1978; Beljaars and Holtslag 1991). Coupled with the fact that the European Centre for Medium-Range Weather Forecasts (ECMWF) operational model currently uses the stability function of Beljaars and Holtslag (1991) (ECMWF 2013), we chose to analyze both the Holtslag and De Bruin (1988) functions and the revised formulation suggested by Beljaars and Holtslag (1991), which does not assume a unit Prandtl number. The functions of Holtslag and De Bruin (1988) imply $\mathrm{Ri}_c = 1.43$, while the Beljaars and Holtslag (1991) functions do not have a critical Richardson number.

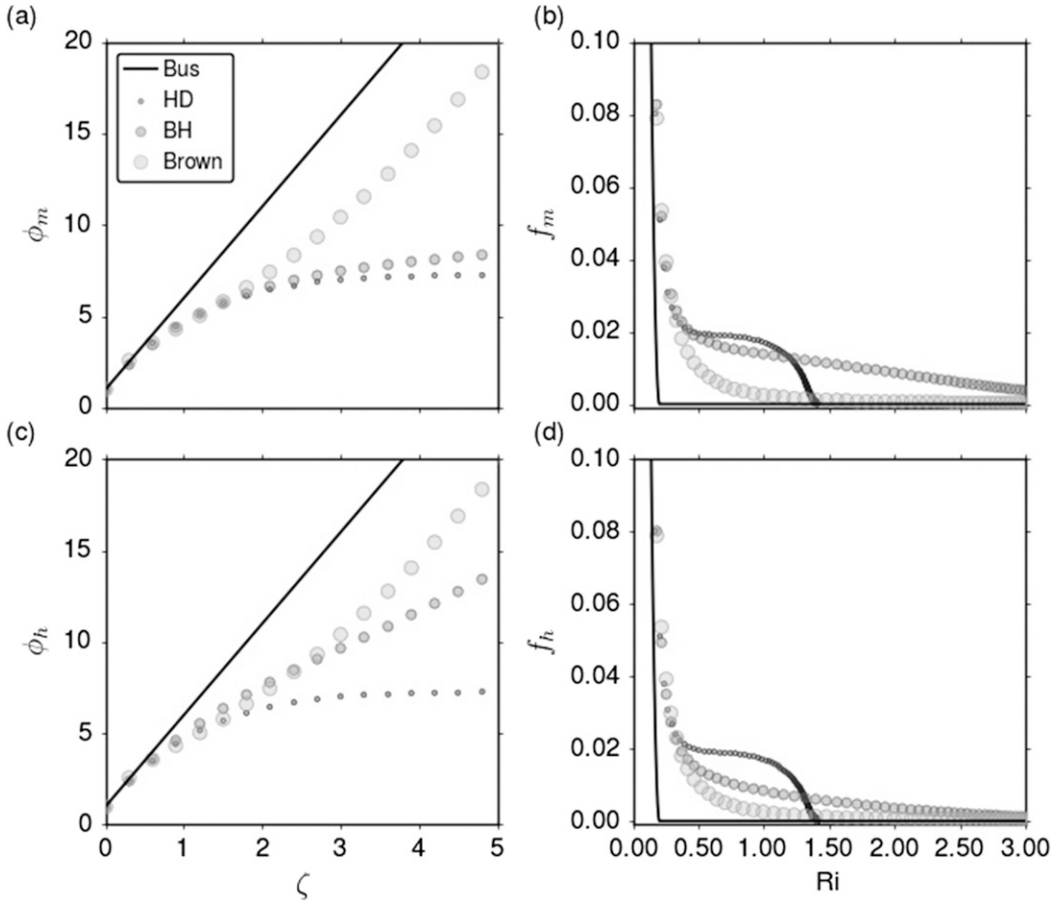

FIG. 2. (a),(c) Similarity functions are shown for Businger et al. (1971) (Bus), Holtslag and De Bruin (1988) (HD), Beljaars and Holtslag (1991) (BH) and Brown et al. (2008) (Brown). (b),(d) The stability functions of (a) and (c), respectively. Corresponding formulas are given in Table 1.

Finally, we also considered the stability function introduced by Brown et al. (2008), characterized by a unit Prandtl number. Although there is no Ri_c for this function, Ri decreases rapidly with increasing stability. This parameterization has been tuned to improve predictions by the Met Office (UKMO) Unified Model [e.g., cloud coverage and thickness (Price et al. 2015)].

Part of the rationale for the consideration of these parameterizations is their use in current operational models. The Businger–Dyer form with $\alpha = 12$ (Delage 1997) is used in the Canadian Meteorological Centre (CMC) Global Deterministic Prediction System (GDPS), the Beljaars and Holtslag (1991) form in the ECMWF operational model, and the Brown et al. (2008) form in the UKMO Unified Model.

3. Equilibrium and linear stability

To examine the linear stability properties of the system, Eqs. (1)–(5) were linearized around the equilibrium solution. Also, the coordinates and state variables were nondimensionalized as

$$\hat{z} = \frac{z}{h}, \quad \hat{t} = \frac{\kappa u_{*\mathrm{eq}} t}{h}, \quad \hat{U} = \frac{U}{u_{*\mathrm{eq}}}, \quad \hat{T} = \frac{T}{T_{*\mathrm{eq}}}. \tag{9}$$

As described in the appendix, the relationship between friction velocity u_* and heat flux H_0 in equilibrium is given implicitly by the following equation, which is Eq. (6) in integrated form [and which also follows from Eqs. (3) and (8) using our parameterized form of K_m]:

$$\int_{z_0/L}^{h/L} \frac{1}{\zeta} \phi_m(\zeta)\, d\zeta = \frac{\ln(h/z_0)}{\hat{u}_*}, \tag{10}$$

where the nondimensional turbulent stress is $\hat{u}_* = u_*/u_{*N}$ and $u_{*N} = \kappa U_h/\ln(h/z_0)$. We define the nondimensional heat flux

$$\hat{H} = \frac{H_0}{u_{*N}^3} \frac{\kappa g}{\rho c_p T_h} \frac{h - z_0}{\ln(h/z_0)}. \tag{11}$$

The definition of $\hat{H}$ differs slightly from the nondimensional heat flux considered by Van de Wiel et al. (2007), which included the critical Richardson number α^{-1} for the Businger et al. (1971) stability function. Equations (10) and (11) can be combined to yield an ordinary differential equation for $\hat{H}$ as a function of $\hat{u}_*$ (derived in the appendix). This ODE can be solved analytically for the Businger–Dyer stability function but must be solved numerically for the other functions under consideration. Knowing $\hat{u}_*$ and $\hat{H}$ in equilibrium, the equilibrium U and T profiles can be obtained.

Linear stability analysis considers the dynamical system

$$\frac{dY}{dt} = AY, \tag{12}$$

where A is the dynamical operator linearized around the equilibrium state, and Y is a continuous function. Classical linear instability analysis assesses the eigenstructure of A to determine the existence of exponentially growing modes.

Letting $\hat{U} = \hat{U}_{\rm eq} + \hat{U}'$ and $\hat{T} = \hat{T}_{\rm eq} + \hat{T}'$ (where the subscript eq denotes the equilibrium values) and linearizing the nondimensionalized Couette flow equations around $(U_{\rm eq}, T_{\rm eq})$ yields

$$\partial_{\hat{t}}\hat{U}' = \partial_{\hat{z}}[F_1(\hat{z}, \hat{L}_{\rm eq})\partial_{\hat{z}}\hat{U}'] + \partial_{\hat{z}}[F_2(\hat{z}, \hat{L}_{\rm eq})\partial_{\hat{z}}\hat{T}'] \tag{13}$$

and

$$\partial_{\hat{t}}\hat{T}' = \partial_{\hat{z}}[F_3(\hat{z}, \hat{L}_{\rm eq})\partial_{\hat{z}}\hat{U}'] + \partial_{\hat{z}}[F_4(\hat{z}, \hat{L}_{\rm eq})\partial_{\hat{z}}\hat{T}'], \tag{14}$$

where

$$F_1(\hat{z}, \hat{L}_{\rm eq}) = 2\hat{z}\phi_m(\hat{z}/\hat{L}_{\rm eq})[f_m({\rm Ri}_{\rm eq}) - {\rm Ri}_{\rm eq}\partial_{\hat{z}}f_m({\rm Ri}_{\rm eq})],$$

$$F_2(\hat{z}, \hat{L}_{\rm eq}) = \hat{z}\frac{\hat{z}}{\hat{L}_{\rm eq}}\partial_{\hat{z}}f_m({\rm Ri}_{\rm eq}),$$

$$F_3(\hat{z}, \hat{L}_{\rm eq}) = \hat{z}\phi_h(\hat{z}/\hat{L}_{\rm eq})[f_h({\rm Ri}_{\rm eq}) - 2{\rm Ri}_{\rm eq}\partial_{\hat{z}}f_h({\rm Ri}_{\rm eq})], \quad \text{and}$$

$$F_4(\hat{z}, \hat{L}_{\rm eq}) = \hat{z}\phi_m(\hat{z}/\hat{L}_{\rm eq})[f_h({\rm Ri}_{\rm eq}) + {\rm Ri}_{\rm eq}\partial_{\hat{z}}f_h({\rm Ri}_{\rm eq})].$$

The boundary conditions are

$$\hat{U}'(\hat{z}_0) = \hat{U}'(1) = \hat{T}'(1) = 0 \tag{15}$$

and, at $z = z_0$,

$$F_3(\hat{z}_0, \hat{L}_{\rm eq})\partial_{\hat{z}}\hat{U}' + F_4(\hat{z}_0, \hat{L}_{\rm eq})\partial_{\hat{z}}\hat{T}' = 0. \tag{16}$$

The dynamical stability calculation finds the eigenmodes of the discretized matrix operator **A** on the right-hand side of Eqs. (13) and (14) with boundary conditions given by Eqs. (15) and (16). For this calculation, the equations were discretized with a Chebyshev grid in the vertical: $z_j = \cos(\pi j/N)$ for $j = 0, 1, \ldots, N$ (Trefethen 2000). The nonuniform structure of the Chebyshev grid, with a high density of points near the upper and lower boundaries, facilitates the polynomial approximations of functions and their derivatives to achieve a higher-order accuracy than the uniform finite-difference grid with the same number of points.

For each of the stability functions presented in Table 1 and a range of $\hat{z}_0$ values, we computed equilibrium curves from Eqs. (A7) and (A8) numerically using a level-4 Runge–Kutta scheme. Linear stability analysis around these curves was performed using Linear Algebra Package (LAPACK) routines in Python (Jones et al. 2001; Strang 1976). For most cases, convergence was apparent by $N = 100$, but for $\hat{z}_0 = 1 \times 10^{-5}$ convergence did not occur until $N = 500$. In consequence, we used $N = 500$ for all of the results shown here.

Numerical simulations of the fully nonlinear Couette flow equations were performed using finite differences in space and time on a logarithmically spaced grid ranging from z_0 to $h = 25$ m. The vertical grid points were set at $z_j = \Delta z_0[(r^j - 1)/(r - 1)]$ with a stretch factor $r = \Delta z_j/\Delta z_{j-1} \simeq 1.05$ and an initial step size of $\Delta z_0 = 0.01$. This stretched grid with 100 vertical levels was used to resolve the approximately logarithmic layer just above $z = z_0$. Time was stepped forward using a level-4 Runge–Kutta scheme with $\Delta t = 0.001$ s.

4. Results

The equilibrium curves relating $\hat{u}_*$ to $\hat{H}$ were computed using the relationship in Eq. (10) for each of the stability functions considered (Figs. 3a, 4a, 5a, 6a). For the Businger–Dyer formulation, we show equilibrium curves for three different values of the parameter α [corresponding to the values used in Van de Wiel et al. (2007), Pruitt et al. (1973), and Delage (1997)]. When the heat flux is normalized as in Van de Wiel et al. (2007), these curves all collapse into a single curve:

$$\alpha\hat{H} + \hat{u}_*^2 - \hat{u}_*^3 = 0. \tag{17}$$

In broad terms, the equilibrium curves corresponding to the different stability functions exhibit qualitatively similar structures. In all cases, there is a maximum in heat flux for intermediate values of $\hat{u}_*$. However, striking differences in the shapes of the equilibrium curves are apparent. In contrast to the Businger–Dyer-type formulations, the equilibrium structures for the other functions generally depend on $\hat{z}_0$, and the extrema are not necessarily unique. For Couette flow, the MSHF method for predicting turbulent collapse is effective, but

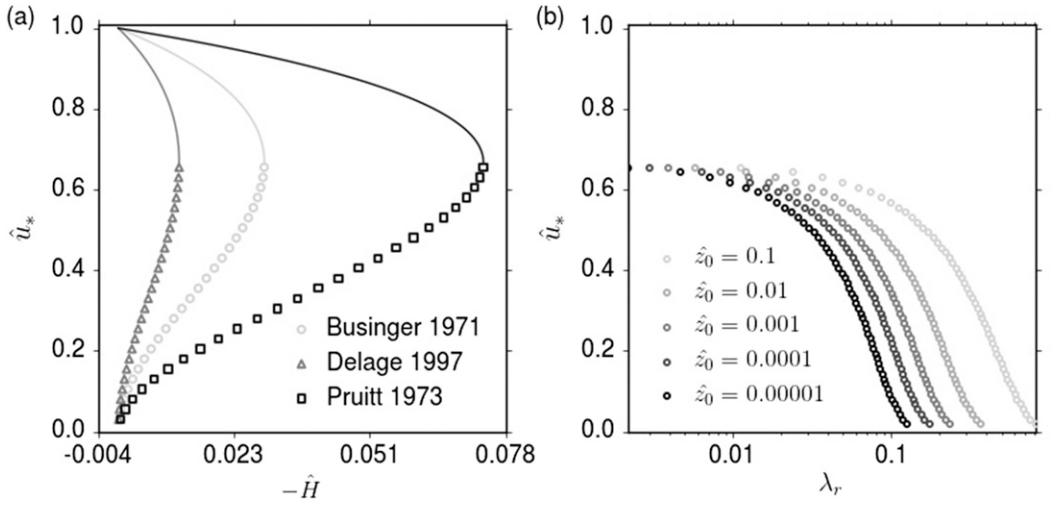

FIG. 3. For the Businger–Dyer-type function (Table 1), (a) the equilibrium diagrams for $\alpha = 2$ (Pruitt et al. 1973), $\alpha = 5$ (Businger et al. 1971; Dyer 1974), and $\alpha = 12$ (Delage 1997) and (b) the maximum real eigenvalue for each $\hat{u}_*$ on the unstable branch are shown. The large open symbols indicate the unstable branch.

the value of the MSHF depends on the choice of parameterization.

The dependence of the nondimensional MSHF $\hat{H}_{\max}$ on the roughness length is illustrated in Fig. 7a. For typical SBL heights of a few tens of meters, the range of z_0 considered corresponds to a range of surface types from flat surfaces like ice and mud to rough urban canopies. The velocity crossing point h may also vary with the roughness scale having less shear over smoother terrain. While $\hat{H}_{\max}$ remains constant for the Businger–Dyer-type functions, it increases with decreasing $\hat{z}_0$ for the other stability functions. The sensitivity of $\hat{H}_{\max}$ to the choice of $\hat{z}_0$ is greatest for relatively small values of $\hat{z}_0$ and relatively weak for larger $\hat{z}_0$.

The value of $\hat{u}_*$ at $\hat{H}_{\max}$ is shown as a function of $\hat{z}_0$ in Fig. 7b. For the Holtslag and De Bruin (1988) and Beljaars and Holtslag (1991) functions, $\hat{u}_*$ decreases with increasing $\hat{z}_0$ for $\hat{z}_0 \lessapprox 0.001$ and increases with increasing $\hat{z}_0$ for larger $\hat{z}_0$. The discontinuity in this structure is explained by the existence of multiple extrema. As shown in Figs. 4b and 5b, at intermediate values of $\hat{z}_0$ the equilibrium curves for these functions exhibit extrema at two different values of $\hat{u}_*$ with close values of $\hat{H}_{\max}$. For larger $\hat{z}_0$, the upper extremum was the global extremum, while for relatively smaller $\hat{z}_0$, the lower extremum was the global extremum.

To assess the linear stability of the equilibrium states, for each $\hat{u}_*$, we considered the eigenvalue with the

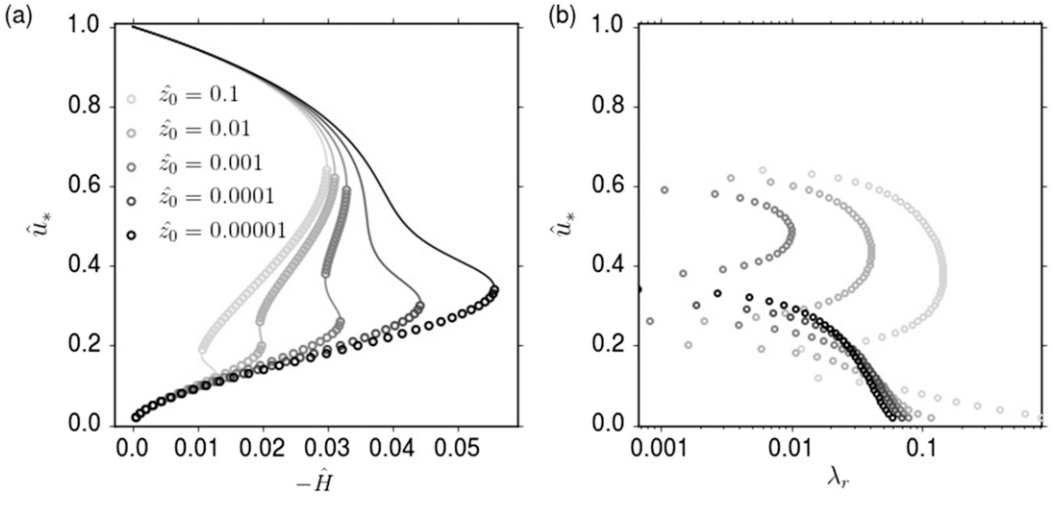

FIG. 4. As in Fig. 3, but for the Holtslag and De Bruin (1988) function (Table 1).

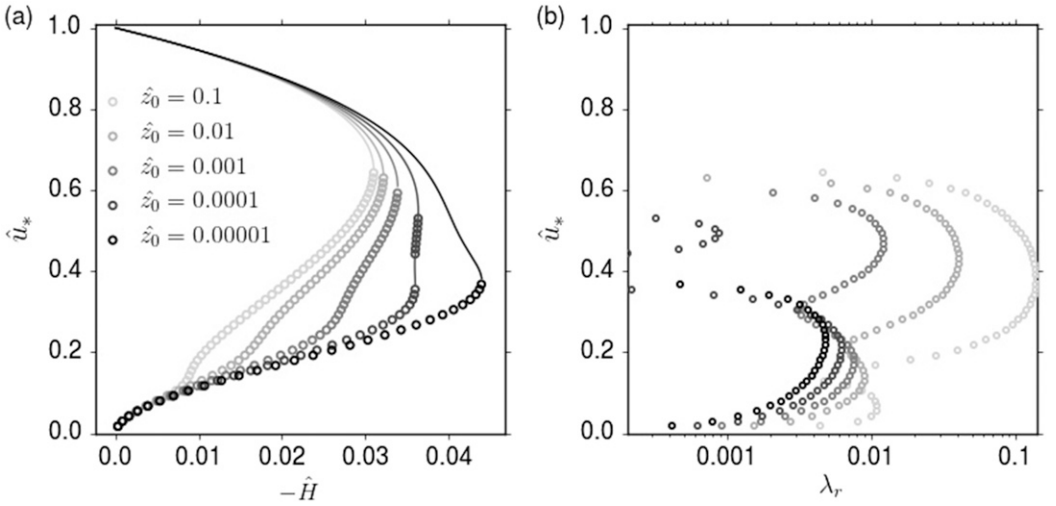

FIG. 5. As in Fig. 3, but for the Beljaars and Holtslag (1991) function (Table 1).

largest real part λ_r. For all stability functions considered, each point on the unstable branch had only one positive real eigenvalue and, therefore, a single unstable eigenmode. This result is invariant to changes in N (the resolution). Even though the branch is unstable, a specific set of conditions is required to excite the unstable mode, meaning that it is possible for unstable equilibrium to persist for long periods of time if those conditions are not met. This fact may be related to the observation that data from Cabauw occupy the unstable branch (Monahan et al. 2015).

The value of the unstable eigenmode λ_r is shown as a function of $\hat{u}_*$ in Figs. 3b, 4b, 5b, and 6b, and the regions of stability on the equilibrium curves are illustrated in Figs. 3a, 4a, 5a, and 6a. Transitions between stable and unstable equilibria are observed to occur at local extrema of the equilibrium curve. Although the equilibrium curve and the boundary between stable and unstable equilibria are insensitive to $\hat{z}_0$ for Businger–Dyer-type functions, the growth rate of the unstable mode depends on $\hat{z}_0$, meaning that the length of time the unstable branch is occupied depends on the surface roughness. Furthermore, the eigenstructure for all of the functions is dependent on $\hat{z}_0$. In the presence of multiple extrema we find multiple regions of stability and instability. For the Holtslag and De Bruin (1988) function in Fig. 4a, there are two unstable branches for $\hat{z}_0 = 0.1, 0.01$, and 0.001. Similarly, for the Beljaars and Holtslag (1991) function, Fig. 5a shows two stable–unstable transitions when $\hat{z}_0 = 0.0001$.

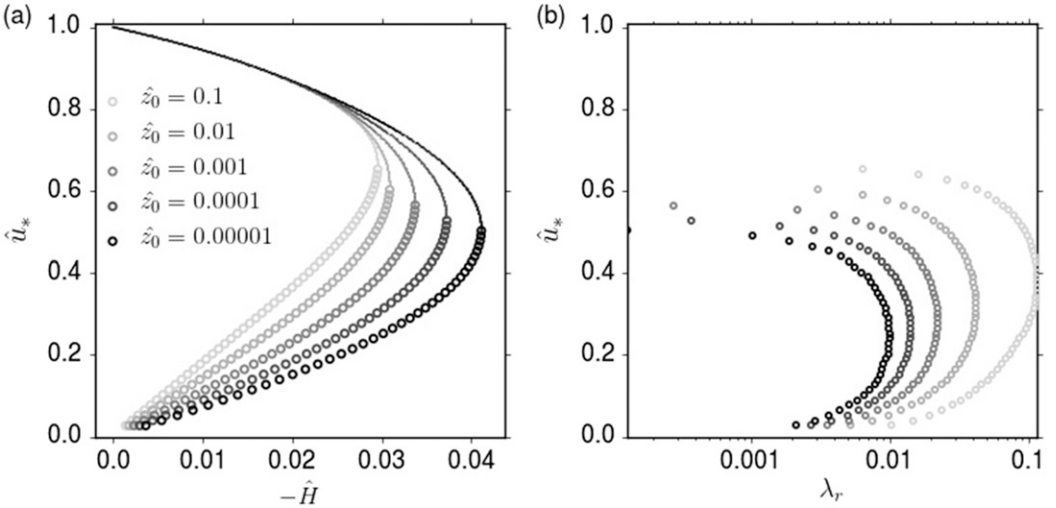

FIG. 6. As in Fig. 3, but for the Brown et al. (2008) function (Table 1).

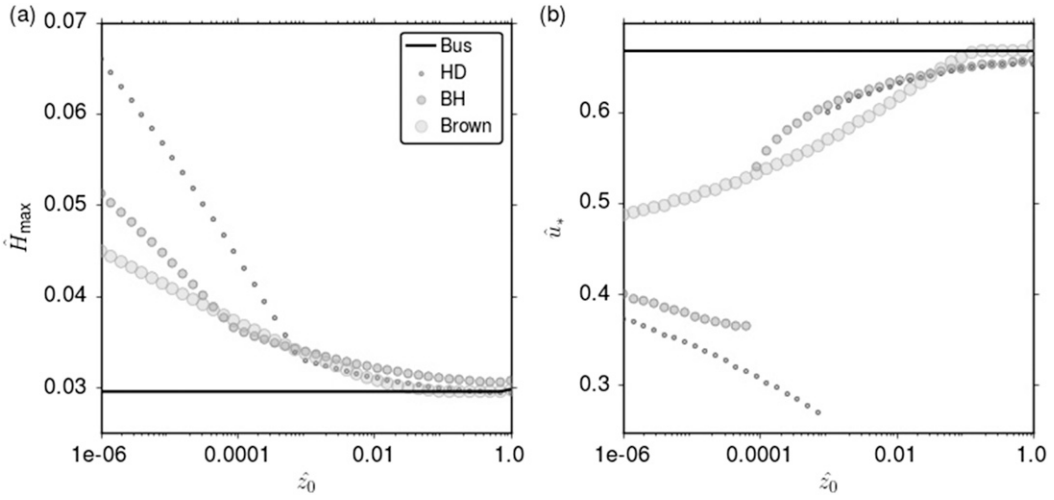

FIG. 7. (a) The MSHF and (b) corresponding u_* as a function of the roughness scale for the stability functions considered.

Linearized stability analysis is a useful tool for understanding the stability properties of a dynamical system, but it is not always sufficient. For example, it fails to predict the onset of turbulence in some classical flows (including Couette and Poiseuille flows). This failure can be attributed to the nonnormality of the governing operator (Gustavsson 1991; Farrell and Ioannou 1993; Reddy and Henningson 1993; Baggett et al. 1995; Trefethen et al. 1993; Farrell and Ioannou 1993). For the discretized Couette flow system, $\mathbf{A}$ is a nonnormal matrix ($\mathbf{A}\mathbf{A}^{\mathrm{T}} \neq \mathbf{A}^{\mathrm{T}}\mathbf{A}$). Because nonnormal systems have eigenvectors that are not orthogonal, growth processes may be influenced by interaction between two or more discrete nonorthogonal modes. Hence, the initial conditions may be amplified by arbitrarily large factors (Trefethen et al. 1993). The modal spectrum determines stability in the ($t \to \infty$) limit. However, generalized stability theory is required to determine stability properties over a finite time (the $t \to 0$ limit). This nonmodal analysis was applied to find the instantaneous growth rates by finding the maximum eigenvalue of $(\mathbf{A} + \mathbf{A}^{\mathrm{T}})/2$ (Farrell and Ioannou 1996).

Nonnormal growth rates for the Businger–Dyer-type function with $\alpha = 5$ are shown in Fig. 8. Growth rates are similar on either side of the bifurcation point. Away from this transition point, growth rates on the unstable branch are significantly larger than those on the stable branch. Likewise, all of the turbulence flux parameterizations had many large real eigenvalues (relative to the growth rates of linear instabilities) for each u_* (not shown). Therefore, even for points on the stable branch(es), transient growth of perturbations is possible over finite time scales. If these perturbations grow large enough, they have the potential to trigger nonlinearities that can alter the behavior of the system.

To better understand the physical relevance of the instabilities along the unstable branch, we compute the dimensional e-folding times $t_e = h/\lambda_r \kappa u_{*\mathrm{eq}}$ and compare these to the time scales on which stable stratification is maintained. If, for example, the e-folding time scale is much longer than the course of the night, then this instability mechanism would not be expected to be relevant to the nocturnal boundary layer. Dimensional

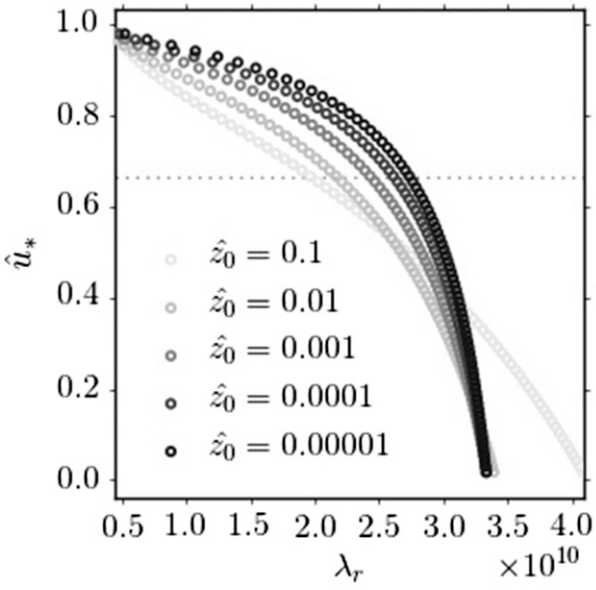

FIG. 8. The maximum real eigenvalue of $(\mathbf{A} + \mathbf{A}^{\mathrm{T}})/2$ for the Businger–Dyer type, demonstrating the possibility of transient growth of perturbations.

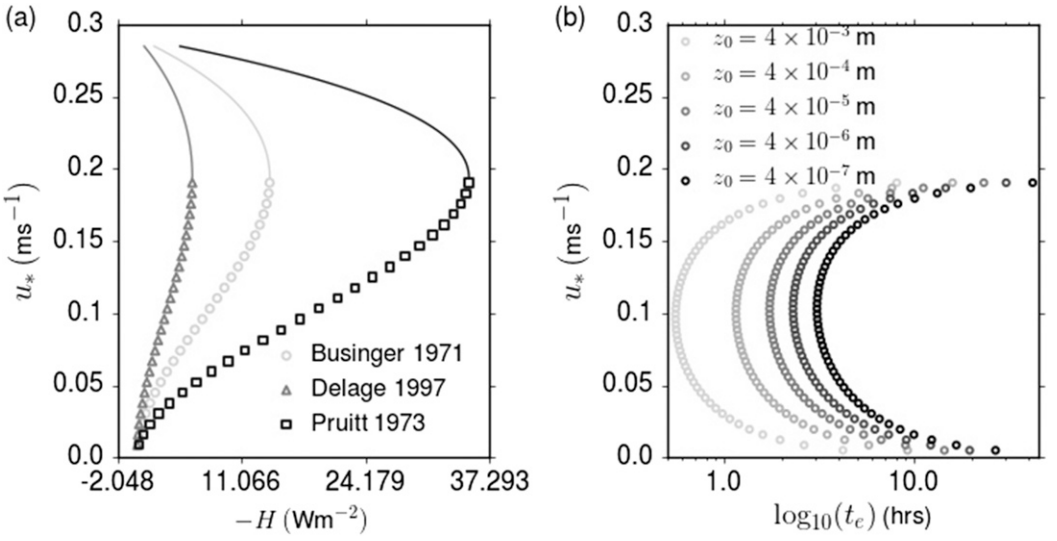

FIG. 9. Dimensional versions of the results shown in Fig. 3 obtained using $h = 25$ m.

values for Fig. 3 are shown in Fig. 9. As the model is highly simplified, the precise value of the growth rates in Fig. 3a is not as important as their order of magnitude. The time scales exhibit larger t_e for smaller z_0, meaning that instabilities take longer to dominate for flows over relatively smooth surfaces. Over relatively rough surfaces t_e typically varied from $O(1)$ to $O(10)$ h, which is comparable to the length of the night, particularly for large z_0, and is certainly relevant to the length of the polar night. Moreover, the growth rates found for the other stability functions were generally on the same order of magnitude.

For a better understanding of how well the nonlinear dynamical system is represented by our linear stability analysis, we simulated Eqs. (1) and (2) numerically using the Businger–Dyer ($\alpha = 5$) function with $z_0 = 0.1$. After verifying the equilibrium solution, we tested a series of random perturbations around it. The form of the initial perturbation is represented by $\sum_{i=1}^{n} \alpha_i e^{\lambda_i t} \mathbf{v}_i$ for eigenvalues λ_i and eigenvectors $\mathbf{v}_i$ of the matrix $\mathbf{A}$. Using the time-stepping model, we investigated the growth of initial perturbations of finite size. Interpolation between the Chebyshev grid and the logarithmic grid was performed using inverse distance weighting. If the coefficient corresponding to the unstable mode was nonzero, perturbation growth eventually dominated. As expected, the amount of time it took to move away from the unstable equilibrium depended on the initial conditions.

The time it took for turbulence to collapse was less than an hour for some perturbations, while for others it was on the order of tens of hours. We verified that the initial growth rates were consistent with the predictions of our linear stability analysis λ_r for both linear and fully nonlinear models. The rapid collapse of turbulence likely occurred because the domain in which the linearization is valid is relatively small.

5. Physical interpretation and conclusions

Although the Couette flow model is an oversimplification of atmospheric boundary layers, it serves as a useful heuristic tool for examining turbulent collapse in the SBL. Using specific closure assumptions, Van de Wiel et al. (2007) demonstrated that the collapse of turbulence could be explained as a linear instability of the system associated with the existence of an MSHF. The clustering of observed turbulence data around the equilibrium curve predicted by the Van de Wiel et al. (2007) model observed in Monahan et al. (2015), including around the unstable branch, motivated a more detailed analysis of the stability characteristics of the model and the sensitivity of its equilibrium structure to turbulence closure assumptions. We extended this analysis by testing a range of turbulence parameterizations (Table 1) and performed a full linear stability analysis to investigate the details of the equilibrium solutions.

The MSHF framework for predicting turbulent collapse, as proposed by Van de Wiel et al. (2007), provides a physical explanation of the transition from the WSBL to the VSBL. Our analysis demonstrated that this framework (Van de Wiel et al. 2012b, 2007; Van Hooijdonk et al. 2015) is robust to substantial changes in the representation of turbulence within the model. However, both the MSHF and the shape of the equilibrium curve varied among the different turbulent flux parameterizations. In particular, for some schemes the

local extrema of the equilibrium curves were not unique. With the exception of the Businger–Dyer-type formulations, both qualitative and quantitative features of the equilibrium curves varied with z_0. The z_0 dependence is a consequence of the linear dependence of the Businger–Dyer similarity functions on ζ and the associated form of the nondimensionalized heat flux. Thus, there were substantial quantitative differences, even though the MSHF framework was not qualitatively sensitive to changes in the parameterization.

Using a Businger–Dyer-type parameterization of turbulent fluxes (Businger et al. 1971; Dyer 1974), Van de Wiel et al. (2007, 2012b) derived an analytical expression for the maximum equilibrium sustainable heat flux and showed that this framework predicted turbulent collapse for both Couette and pressure-driven flows. Equivalently, the MSHF framework can be expressed in terms of the speed at a given altitude. A specified surface heat flux determines a characteristic velocity scale $U_{\min}$ (Van de Wiel et al. 2012b) that represents the minimum wind speed needed to sustain turbulence. Normalizing the wind speed with this quantity, Van Hooijdonk et al. (2015) defined the shear capacity $\mathrm{SC} = U/U_{\min}$ that would separate the WSBL from the VSBL at $U/U_{\min} = 1$. Our results indicate that the value of the MSHF depends on the parameterization of turbulent fluxes within the model. As a result of the dependence of the MSHF on z_0, we expect the choice of parameterization to affect the equation for the MSHF and, in turn, the equation for $U_{\min}$. The influence of the choice of parameterization is tempered by the fact that $U_{\min}$ depends on the cube root of the MSHF. Transitions from the WSBL to the VSBL can be predicted using the MSHF and shear capacity approaches, but care should be taken to calculate these values with the appropriate stability function.

Linear stability analysis showed that, for all of the stability functions considered here, the stability properties depend on $\hat{z}_0$, and the change of stability between stable and unstable solutions occurred at the local extrema of the equilibrium curve. As a result, some of the parameterizations exhibited disjointed regions of stability.

For each $\hat{u}_*$ on the unstable branch, there was only one unstable eigenmode and the time scales of turbulent collapse are typically on the order of 1–10 h. These facts could explain why observations indicate that the unstable branch is populated by observations from Cabauw (Monahan et al. 2015). If there were many unstable modes or if the growth rate was much faster, then we would expect these points to rapidly move away from the unstable branch. Instead, the existence of a single unstable mode implies that a specific set of conditions is necessary to elicit the growth of perturbations that would drive the trajectory of solutions away from the unstable branch. However, this is not the only possible reason for the population of the unstable branch. Another contributing factor could be the existence of intermittent turbulent bursts characteristic of the VSBL (Mahrt 2014), which are not included in this model. Finally, generalized stability analysis demonstrated that, even around the stable branch, the system is susceptible to transient growth of disturbances over short times.

While the Couette model provides a heuristic description of the transition from the WSBL to the VSBL, it cannot account for the reverse transition. A complete understanding of transitions from the VSBL to the WSBL requires a more comprehensive model. Recent work has focused on the role of the pressure gradient force (Donda et al. 2015), but more work is needed to capture the full complexity of this dynamical system (Sun et al. 2002, 2004).

Acknowledgments. The authors acknowledge support by the Natural Sciences and Engineering Research Council of Canada (NSERC). This research was enabled in part by support provided by WestGrid (www.westgrid.ca) and Compute Canada/Calcul Canada (www.computecanada.ca). We also acknowledge helpful comments from Carsten Abraham, Bas van de Wiel, and two anonymous referees.

APPENDIX

Equilibrium Analysis and Linearized Dynamics

In equilibrium, the turbulent momentum and heat fluxes are uniform across the domain. We can use the Monin–Obukhov similarity theory (MOST) to compute a relationship between these turbulent fluxes, assuming a specified wind speed at $z = h$ (Monin and Obukhov 1954). By definition,

$$\int_{z_0}^{h} \partial_z \overline{u}\, dz = \overline{u}(h) - \overline{u}(0) = U_h, \tag{A1}$$

and, using MOST,

$$\int_{z_0}^{h} \partial_z \overline{u}\, dz = \int_{z_0}^{h} \left(\frac{u_*}{\kappa z}\right) \phi_m\left(\frac{z}{L}\right) dz = \frac{u_*}{\kappa} \int_{z_0/L}^{h/L} \frac{1}{\zeta} \phi_m(\zeta)\, d\zeta, \tag{A2}$$

where $\zeta = z/L$ and $\phi_m(\zeta)$ is the Monin–Obukhov similarity function for momentum. Defining the equilibrium friction velocity for neutral stratification

$$u_{*N} = \frac{U_h \kappa}{\ln(h/z_0)}, \tag{A3}$$

we obtain

$$\frac{u_{*N}\ln(h/z_0)}{\kappa}=\frac{u_*}{\kappa}\int_{z_0/L}^{h/L}\frac{1}{\zeta}\phi_m(\zeta)\,d\zeta, \tag{A4}$$

which defines an implicit equation relating u_* to H given by Eq. (10). Alternatively, this equation can be derived by solving for $\partial_z U$ from Eq. (3) using the expression for K_m as well as the relationship between f_m and ϕ_m and then integrating with respect to height. This equation can be transformed into a computationally more tractable form first by writing $\upsilon = h/L$ so that we have

$$\int_{\upsilon z_0/h}^{\upsilon}\frac{1}{\zeta}\phi_m(\zeta)\,d\zeta=\frac{\ln(h/z_0)}{\hat{u}_*}. \tag{A5}$$

Differentiating with respect to $\hat{u}_*$, this becomes

$$\frac{d\upsilon}{d\hat{u}_*}\frac{\phi_m(\upsilon)}{\upsilon}-\frac{z_0}{h}\frac{d\upsilon}{d\hat{u}_*}\frac{\phi_m(\upsilon z_0/h)h}{\upsilon z_0}=-\frac{1}{\hat{u}_*^2}, \tag{A6}$$

from which we obtain

$$\frac{d\upsilon}{d\hat{u}_*}=-\frac{\ln(h/z_0)}{\hat{u}_*^2}\frac{\upsilon}{\phi_m(\upsilon)-\phi_m(\upsilon z_0/h)}. \tag{A7}$$

Equation (A7) is an ordinary differential equation for υ as a function of u_*, with initial (rather, final) condition

$$\upsilon(\hat{u}_*=1)=0 \tag{A8}$$

(as $1/L = 0$ in neutral stratification). Solving this equation for υ, the normalized heat flux $\hat{H}$ [Eq. (11)] can then be calculated. In general, this solution can only be found numerically. For the special case of the Businger–Dyer-type similarity functions, the solution is

$$\hat{u}_*^3-\hat{u}_*^2-\alpha\hat{H}=0, \tag{A9}$$

with $\hat{H}$ given by Eq. (11) (Van de Wiel et al. 2007).

For the linear stability analysis, we need to start with Eqs. (1) and (2) and apply the parameterizations given by Eqs. (3) and (4). Allowing for arbitrary similarity functions for momentum and heat fluxes, we have

$$\partial_t U=\partial_z[(\kappa z)^2(\partial_z U)^2 f_m(\mathrm{Ri})] \quad \text{and} \tag{A10}$$

$$\partial_t T=\partial_z[(\kappa z)^2(\partial_z U)(\partial_z T)f_h(\mathrm{Ri})], \tag{A11}$$

where Ri is given by Eq. (5).

Splitting U and T into equilibrium and perturbation parts, we have

$$\mathrm{Ri}=\frac{g}{T_h}\frac{\partial_z(T_{\mathrm{eq}}+T')}{(\partial_z U_{\mathrm{eq}}+\partial_z U')^2} \quad \text{and} \tag{A12}$$

$$\simeq \mathrm{Ri}_{\mathrm{eq}}+\mathrm{Ri}_{\mathrm{eq}}\frac{\partial_z T'}{\partial_z T_{\mathrm{eq}}}-2\mathrm{Ri}_{\mathrm{eq}}\frac{\partial_z U'}{\partial_z U_{\mathrm{eq}}}. \tag{A13}$$

For sufficiently small perturbations, it follows that

$$f_m(\mathrm{Ri})\simeq f_m(\mathrm{Ri}_{\mathrm{eq}})+[\mathrm{Ri}_{\mathrm{eq}}D_{\mathrm{Ri}}f_m(\mathrm{Ri}_{\mathrm{eq}})]\frac{\partial_z T'}{\partial_z T_{\mathrm{eq}}}-2[\mathrm{Ri}_{\mathrm{eq}}D_{\mathrm{Ri}}f_m(\mathrm{Ri}_{\mathrm{eq}})]\frac{\partial_z U'}{\partial_z U_{\mathrm{eq}}}. \tag{A14}$$

The same expression holds for $f_m(\mathrm{Ri})$, where D_{Ri} indicates the differential operator $d/d\mathrm{Ri}$. It follows that (to first order in the perturbations)

$$(\partial_z U)^2 f_m(\mathrm{Ri})\simeq(\partial_z U_{\mathrm{eq}})^2 f_m(\mathrm{Ri}_{\mathrm{eq}})+2(\partial_z U_{\mathrm{eq}})[f_m(\mathrm{Ri}_{\mathrm{eq}})-\mathrm{Ri}_{\mathrm{eq}}D_{\mathrm{Ri}}f_m(\mathrm{Ri}_{\mathrm{eq}})]\partial_z U'+\frac{(\partial_z U_{\mathrm{eq}})^2}{\partial_z T_{\mathrm{eq}}}[\mathrm{Ri}_{\mathrm{eq}}D_{\mathrm{Ri}}f_m(\mathrm{Ri}_{\mathrm{eq}})]\partial_z T' \tag{A15}$$

and

$$(\partial_z U)(\partial_z T)f_h(\mathrm{Ri})\simeq(\partial_z U_{\mathrm{eq}})(\partial_z T_{\mathrm{eq}})f_h(\mathrm{Ri}_{\mathrm{eq}})+(\partial_z T_{\mathrm{eq}})[f_h(\mathrm{Ri}_{\mathrm{eq}})-2\mathrm{Ri}_{\mathrm{eq}}D_{\mathrm{Ri}}f_h(\mathrm{Ri}_{\mathrm{eq}})]\partial_z U'+(\partial_z U_{\mathrm{eq}})[f_h(\mathrm{Ri}_{\mathrm{eq}})+\mathrm{Ri}_{\mathrm{eq}}D_{\mathrm{Ri}}f_h(\mathrm{Ri}_{\mathrm{eq}})]\partial_z T'. \tag{A16}$$

These results lead to the general perturbation equation:

$$\partial_t U'=\partial_z\{2(\kappa z)^2(\partial_z U_{\mathrm{eq}})[f_m(\mathrm{Ri}_{\mathrm{eq}})-\mathrm{Ri}_{\mathrm{eq}}D_{\mathrm{Ri}}f_m(\mathrm{Ri}_{\mathrm{eq}})]\partial_z U'\}+\partial_z\left[(\kappa z)^2\frac{g}{T_h}D_{\mathrm{Ri}}f_m(\mathrm{Ri}_{\mathrm{eq}})\partial_z T'\right] \tag{A17}$$

$$\partial_t T'=\partial_z\{(\kappa z)^2(\partial_z T_{\mathrm{eq}})[f_h(\mathrm{Ri}_{\mathrm{eq}})-2\mathrm{Ri}_{\mathrm{eq}}D_{\mathrm{Ri}}f_h(\mathrm{Ri}_{\mathrm{eq}})]\partial_z U'\}+\partial_z\{(\kappa z)^2(\partial_z U_{\mathrm{eq}})[f_h(\mathrm{Ri}_{\mathrm{eq}})+\mathrm{Ri}_{\mathrm{eq}}D_{\mathrm{Ri}}f_h(\mathrm{Ri}_{\mathrm{eq}})]\partial_z T'\}, \tag{A18}$$

with the following boundary conditions:

$$U'(z_0) = U'(h) = 0, \quad T'(h) = 0, \quad H'(z_0) = 0, \tag{A19}$$

where $H = (\kappa z)^2(\partial_z U)(\partial_z T) f_h(\mathrm{Ri})$. From Eq. (A16), it follows that the fourth boundary condition is

$$0 = (\partial_z T_{\mathrm{eq}})[f_h(\mathrm{Ri}_{\mathrm{eq}}) - 2\mathrm{Ri}_{\mathrm{eq}} D_{\mathrm{Ri}} f_h(\mathrm{Ri}_{\mathrm{eq}})]\partial_z U' + (\partial_z U_{\mathrm{eq}})[f_h(\mathrm{Ri}_{\mathrm{eq}}) + \mathrm{Ri}_{\mathrm{eq}} D_{\mathrm{Ri}} f_h(\mathrm{Ri}_{\mathrm{eq}})]\partial_z T' \tag{A20}$$

at $z = z_0$.

Using Eqs. (8) and the fact that $\mathrm{Ri}_{\mathrm{eq}} = \zeta\phi_h(\zeta)/\phi_m^2(\zeta)$, we can also write

$$\begin{aligned} D_{\mathrm{Ri}} f_m(\mathrm{Ri}_{\mathrm{eq}}) &= -\frac{2}{\phi_m^3} D_{\mathrm{Ri}}\phi_m \\ &= -\frac{2D_\zeta\phi_m}{\phi_m^3} D_{\mathrm{Ri}}\zeta \\ &= -\frac{2D_\zeta\phi_m}{\phi_m\phi_h + \zeta D_\zeta\phi_h\phi_m - 2\zeta\phi_h D_\zeta\phi_m} \end{aligned}$$

and

$$D_{\mathrm{Ri}} f_h(\mathrm{Ri}_{\mathrm{eq}}) = -\frac{\phi_m^2}{\phi_h}\left(\frac{D_\zeta\phi_h}{\phi_h} + \frac{D_\zeta\phi_m}{\phi_m}\right)\frac{1}{\phi_m\phi_h + \zeta D_\zeta\phi_h\phi_m - 2\zeta\phi_h D_\zeta\phi_m}.$$

The equilibrium profile given by Eq. (10) depends on only the momentum similarity function ϕ_m (or stability function f_m), but the stability properties that arise from the linearization [Eqs. (13) and (14)] depend on the functions for both momentum and heat. As a result, the behavior of the turbulent Prandtl number is irrelevant to the equilibrium structure but affects the stability properties.

REFERENCES

Andreas, E. L, 2002: Parameterizing scalar transfer over snow and ice: A review. *J. Hydrometeor.*, **3**, 417–432, doi:10.1175/1525-7541(2002)003<0417:PSTOSA>2.0.CO;2.

Arya, S. P., 1999: *Air Pollution Meteorology and Dispersion*. Oxford University Press, 320 pp.

Baggett, J. S., T. A. Driscoll, and L. N. Trefethen, 1995: A mostly linear model of transition to turbulence. *Phys. Fluids*, **7**, 833–838, doi:10.1063/1.868606.

Banta, R. M., L. Mahrt, D. Vickers, J. Sun, B. B. Balsley, Y. L. Pichugina, and E. J. Williams, 2007: The very stable boundary layer on nights with weak low-level jets. *J. Atmos. Sci.*, **64**, 3068–3090, doi:10.1175/JAS4002.1.

Basu, S., A. A. Holtslag, B. J. Van De Wiel, A. F. Moene, and G.-J. Steeneveld, 2008: An inconvenient truth about using sensible heat flux as a surface boundary condition in models under stably stratified regimes. *Acta Geophys.*, **56**, 88–99, doi:10.2478/s11600-007-0038-y.

Beljaars, A. C. M., and A. A. M. Holtslag, 1991: Flux parameterization over land surfaces for atmospheric models. *J. Appl. Meteor.*, **30**, 327–341, doi:10.1175/1520-0450(1991)030<0327:FPOLSF>2.0.CO;2.

Brown, A., R. Beare, J. Edwards, A. Lock, S. Keogh, S. Milton, and D. Walters, 2008: Upgrades to the boundary-layer scheme in the Met Office Numerical Weather Prediction model. *Bound.-Layer Meteor.*, **128**, 117–132, doi:10.1007/s10546-008-9275-0.

Businger, J. A., J. C. Wyngaard, Y. Izumi, and E. F. Bradley, 1971: Flux-profile relationships in the atmospheric surface layer. *J. Atmos. Sci.*, **28**, 181–189, doi:10.1175/1520-0469(1971)028<0181:FPRITA>2.0.CO;2.

Carson, D., and P. Richards, 1978: Modelling surface turbulent fluxes in stable conditions. *Bound.-Layer Meteor.*, **14**, 67–81, doi:10.1007/BF00123990.

Chenge, Y., and W. Brutsaert, 2005: Flux-profile relationships for wind speed and temperature in the stable atmospheric boundary layer. *Bound.-Layer Meteor.*, **114**, 519–538, doi:10.1007/s10546-004-1425-4.

Clarke, R., 1970: Observational studies in the atmospheric boundary layer. *Quart. J. Roy. Meteor. Soc.*, **96**, 91–114, doi:10.1002/qj.49709640709.

De Bruin, H., 1994: Analytic solutions of the equations governing the temperature fluctuation method. *Bound.-Layer Meteor.*, **68**, 427–432, doi:10.1007/BF00706800.

Delage, Y., 1997: Parameterising sub-grid scale vertical transport in atmospheric models under statically stable conditions. *Bound.-Layer Meteor.*, **82**, 23–48, doi:10.1023/A:1000132524077.

Derbyshire, S., 1999: Boundary-layer decoupling over cold surfaces as a physical boundary-instability. *Bound.-Layer Meteor.*, **90**, 297–325, doi:10.1023/A:1001710014316.

Donda, J., I. van Hooijdonk, A. Moene, H. Jonker, G. van Heijst, H. Clercx, and B. van de Wiel, 2015: Collapse of turbulence in stably stratified channel flow: A transient phenomenon. *Quart. J. Roy. Meteor. Soc.*, **141**, 2137–2147, doi:10.1002/qj.2511.

Dyer, A., 1974: A review of flux-profile relationships. *Bound.-Layer Meteor.*, **7**, 363–372, doi:10.1007/BF00240838.

ECMWF, 2013: Part IV: Physical processes. IFS documentation—Cy40r1. ECMWF Tech. Rep. Cy40r1, 190 pp.

Farrell, B. F., and P. J. Ioannou, 1993: Stochastic forcing of the linearized Navier–Stokes equations. *Phys. Fluids*, **5**, 2600–2609, doi:10.1063/1.858894.

——, and ——, 1996: Generalized stability theory. Part I: Autonomous operators. *J. Atmos. Sci.*, **53**, 2025–2040, doi:10.1175/1520-0469(1996)053<2025:GSTPIA>2.0.CO;2.

Fernando, H., and J. Weil, 2010: Whither the stable boundary layer? A shift in the research agenda. *Bull. Amer. Meteor. Soc.*, **91**, 1475–1484, doi:10.1175/2010BAMS2770.1.

Grachev, A. A., C. W. Fairall, P. O. G. Persson, E. L Andreas, and P. S. Guest, 2005: Stable boundary-layer scaling regimes: The SHEBA data. *Bound.-Layer Meteor.*, **116**, 201–235, doi:10.1007/s10546-004-2729-0.

Gustavsson, L. H., 1991: Energy growth of three-dimensional disturbances in plane Poiseuille flow. *J. Fluid Mech.*, **224**, 241–260, doi:10.1017/S002211209100174X.

He, Y., A. H. Monahan, C. G. Jones, A. Dai, S. Biner, D. Caya, and K. Winger, 2010: Probability distributions of land surface wind speeds over North America. *J. Geophys. Res.*, **115**, D04103, doi:10.1029/2008JD010708.

——, N. A. McFarlane, and A. H. Monahan, 2012: The influence of boundary layer processes on the diurnal variation of the

climatological near-surface wind speed probability distribution over land. *J. Climate*, **25**, 6441–6458, doi:10.1175/JCLI-D-11-00321.1.

Hicks, B. B., 1976: Wind profile relationships from the Wangara experiment. *Quart. J. Roy. Meteor. Soc.*, **102**, 535–551, doi:10.1002/qj.49710243304.

Holtslag, A., and H. De Bruin, 1988: Applied modeling of the nighttime surface energy balance over land. *J. Appl. Meteor.*, **27**, 689–704, doi:10.1175/1520-0450(1988)027<0689:AMOTNS>2.0.CO;2.

——, and Coauthors, 2013: Stable atmospheric boundary layers and diurnal cycles: Challenges for weather and climate models. *Bull. Amer. Meteor. Soc.*, **94**, 1691–1706, doi:10.1175/BAMS-D-11-00187.1.

Howell, J., and J. Sun, 1999: Surface-layer fluxes in stable conditions. *Bound.-Layer Meteor.*, **90**, 495–520, doi:10.1023/A:1001788515355.

Jones, E., and Coauthors, 2001: SciPy: Open source scientific tools for Python. Accessed 6 January 2016. [Available online at http://www.scipy.org/.]

Kondo, J., O. Kanechika, and N. Yasuda, 1978: Heat and momentum transfers under strong stability in the atmospheric surface layer. *J. Atmos. Sci.*, **35**, 1012–1021, doi:10.1175/1520-0469(1978)035<1012:HAMTUS>2.0.CO;2.

Mahrt, L., 1985: Vertical structure and turbulence in the very stable boundary layer. *J. Atmos. Sci.*, **42**, 2333–2349, doi:10.1175/1520-0469(1985)042<2333:VSATIT>2.0.CO;2.

——, 1998a: Nocturnal boundary-layer regimes. *Bound.-Layer Meteor.*, **88**, 255–278, doi:10.1023/A:1001171313493.

——, 1998b: Stratified atmospheric boundary layers and breakdown of models. *Theor. Comput. Fluid Dyn.*, **11**, 263–279, doi:10.1007/s001620050093.

——, 2011: The near-calm stable boundary layer. *Bound.-Layer Meteor.*, **140**, 343–360, doi:10.1007/s10546-011-9616-2.

——, 2014: Stably stratified atmospheric boundary layers. *Annu. Rev. Fluid Mech.*, **46**, 23–45, doi:10.1146/annurev-fluid-010313-141354.

Malhi, Y. S., 1995: The significance of the dual solutions for heat fluxes measured by the temperature fluctuation method in stable conditions. *Bound.-Layer Meteor.*, **74**, 389–396, doi:10.1007/BF00712379.

Monahan, A. H., Y. He, N. McFarlane, and A. Dai, 2011: The probability distribution of land surface wind speeds. *J. Climate*, **24**, 3892–3909, doi:10.1175/2011JCLI4106.1.

——, T. Rees, Y. He, and N. McFarlane, 2015: Multiple regimes of wind, stratification, and turbulence in the stable boundary layer. *J. Atmos. Sci.*, **72**, 3178–3198, doi:10.1175/JAS-D-14-0311.1.

Monin, A., and A. Obukhov, 1954: Basic laws of turbulent mixing in the surface layer of the atmosphere. *Contrib. Geophys. Inst. Acad. Sci. USSR*, **151**, 163–187.

Nappo, C. J., 1991: Sporadic breakdowns of stability in the PBL over simple and complex terrain. *Bound.-Layer Meteor.*, **54**, 69–87, doi:10.1007/BF00119413.

Nieuwstadt, F. T. M., 1984: The turbulent structure of the stable, nocturnal boundary layer. *J. Atmos. Sci.*, **41**, 2202–2216, doi:10.1175/1520-0469(1984)041<2202:TTSOTS>2.0.CO;2.

Optis, M., A. Monahan, and F. C. Bosveld, 2015: Limitations and breakdown of Monin–Obukhov similarity theory for wind profile extrapolation under stable stratification. *Wind Energy*, **19**, 1053–1072, doi:10.1002/we.1883.

Pahlow, M., M. B. Parlange, and F. Porté-Agel, 2001: On Monin–Obukhov similarity in the stable atmospheric boundary layer. *Bound.-Layer Meteor.*, **99**, 225–248, doi:10.1023/A:1018909000098.

Petersen, E. L., N. G. Mortensen, L. Landberg, J. Højstrup, and H. P. Frank, 1998: Wind power meteorology. Part I: Climate and turbulence. *Wind Energy*, **1**, 25–45, doi:10.1002/(SICI)1099-1824(199804)1:1+<25::AID-WE4>3.0.CO;2-D.

Price, J., A. Porson, and A. Lock, 2015: An observational case study of persistent fog and comparison with an ensemble forecast model. *Bound.-Layer Meteor.*, **155**, 301–327, doi:10.1007/s10546-014-9995-2.

Pruitt, W., D. Morgan, and F. Lourence, 1973: Momentum and mass transfers in the surface boundary layer. *Quart. J. Roy. Meteor. Soc.*, **99**, 370–386, doi:10.1002/qj.49709942014.

Reddy, S. C., and D. S. Henningson, 1993: Energy growth in viscous channel flows. *J. Fluid Mech.*, **252**, 209–238, doi:10.1017/S0022112093003738.

Salmond, J., and I. McKendry, 2005: A review of turbulence in the very stable nocturnal boundary layer and its implications for air quality. *Prog. Phys. Geogr.*, **29**, 171–188, doi:10.1191/0309133305pp442ra.

Strang, G., 1976: *Linear Algebra and Its Applications*. Academic Press, 385 pp.

Sun, J., and Coauthors, 2002: Intermittent turbulence associated with a density current passage in the stable boundary layer. *Bound.-Layer Meteor.*, **105**, 199–219, doi:10.1023/A:1019969131774.

——, and Coauthors, 2004: Atmospheric disturbances that generate intermittent turbulence in nocturnal boundary layers. *Bound.-Layer Meteor.*, **110**, 255–279, doi:10.1023/A:1026097926169.

Taylor, P., 1971: A note on the log-linear velocity profile in stable conditions. *Quart. J. Roy. Meteor. Soc.*, **97**, 326–329, doi:10.1002/qj.49709741308.

Trefethen, L. N., 2000: *Spectral Methods in MATLAB*. SIAM, 165 pp.

——, A. Trefethen, S. Reddy, and T. Driscoll, 1993: Hydrodynamic stability without eigenvalues. *Science*, **261**, 578–584, doi:10.1126/science.261.5121.578.

Van de Wiel, B. J. H., R. Ronda, A. Moene, H. De Bruin, and A. Holtslag, 2002: Intermittent turbulence and oscillations in the stable boundary layer over land. Part I: A bulk model. *J. Atmos. Sci.*, **59**, 942–958, doi:10.1175/1520-0469(2002)059<0942:ITAOIT>2.0.CO;2.

——, A. F. Moene, G. J. Steeneveld, O. K. Hartogensis, and A. A. M. Holtslag, 2007: Predicting the collapse of turbulence in stably stratified boundary layers. *Flow Turbul. Combust.*, **79**, 251–274, doi:10.1007/s10494-007-9094-2.

——, ——, and H. J. J. Jonker, 2012a: The cessation of continuous turbulence as precursor of the very stable nocturnal boundary layer. *J. Atmos. Sci.*, **69**, 3097–3115, doi:10.1175/JAS-D-12-064.1.

——, ——, ——, P. Baas, S. Basu, J. M. M. Donda, J. Sun, and A. A. M. Holtslag, 2012b: The minimum wind speed for sustainable turbulence in the nocturnal boundary layer. *J. Atmos. Sci.*, **69**, 3116–3127, doi:10.1175/JAS-D-12-0107.1.

Van Hooijdonk, I. G., J. M. Donda, H. J. Clercx, F. C. Bosveld, and B. J. van de Wiel, 2015: Shear capacity as prognostic for nocturnal boundary layer regimes. *J. Atmos. Sci.*, **72**, 1518–1532, doi:10.1175/JAS-D-14-0140.1.

Walters, J. T., R. T. McNider, X. Shi, W. B. Norris, and J. R. Christy, 2007: Positive surface temperature feedback in the stable nocturnal boundary layer. *Geophys. Res. Lett.*, **34**, L12709, doi:10.1029/2007GL029505.

Webb, E. K., 1970: Profile relationships: The log-linear range and extension to strong stability. *Quart. J. Roy. Meteor. Soc.*, **96**, 67–90, doi:10.1002/qj.49709640708.

Williams, A., S. Chambers, and A. Griffiths, 2013: Bulk mixing and decoupling of the nocturnal stable boundary layer characterized using a ubiquitous natural tracer. *Bound.-Layer Meteor.*, **149**, 381–402, doi:10.1007/s10546-013-9849-3.